

# Quantum squeezing amplification with a weak Kerr nonlinear oscillator

Yanyan Cai,<sup>1,2,3,\*</sup> Xiaowei Deng,<sup>2,\*</sup> Libo Zhang,<sup>1,2,3,\*</sup> Zhongchu Ni,<sup>1,2,3,4</sup> Jiasheng Mai,<sup>1,2,3</sup>  
Peihao Huang,<sup>2</sup> Pan Zheng,<sup>2</sup> Ling Hu,<sup>2</sup> Song Liu,<sup>1,2,3,5</sup> Yuan Xu,<sup>2,5,†</sup> and Dapeng Yu,<sup>2,5</sup>

<sup>1</sup>*Shenzhen Institute for Quantum Science and Engineering,  
Southern University of Science and Technology, Shenzhen 518055, China*

<sup>2</sup>*International Quantum Academy, Shenzhen 518048, China*

<sup>3</sup>*Guangdong Provincial Key Laboratory of Quantum Science and Engineering,  
Southern University of Science and Technology, Shenzhen 518055, China*

<sup>4</sup>*Department of Physics, Southern University of Science and Technology, Shenzhen 518055, China*

<sup>5</sup>*Shenzhen Branch, Hefei National Laboratory, Shenzhen 518048, China*

Quantum squeezed states, with reduced quantum noise, have been widely utilized in quantum sensing and quantum error correction applications. However, generating and manipulating these nonclassical states with a large squeezing degree typically requires strong nonlinearity, which inevitably induces additional decoherence that diminishes the overall performance. Here, we demonstrate the generation and amplification of squeezed states in a superconducting microwave cavity with weak Kerr nonlinearity. By subtly engineering an off-resonant microwave drive, we observe cyclic dynamics of the quantum squeezing evolution for various Fock states  $|N\rangle$  with  $N$  up to 6 in displaced frame of the cavity. Furthermore, we deterministically realize quantum squeezing amplification by alternately displacing the Kerr oscillator using the Trotterization technique, achieving a maximum squeezing degree of 14.6 dB and squeezing rate of 0.28 MHz. Our hardware-efficient displacement-enhanced squeezing operations provide an alternative pathway for generating large squeezed states, promising potential applications in quantum-enhanced sensing and quantum information processing.

The landscape of quantum information science has been substantially enriched by the utilization of nonclassical bosonic states, which are essential for continuous variable quantum information processing [1, 2]. Among these states, squeezed states [3], which exhibit reduced noise in one quadrature but increased noise in the conjugate one, stand out for their remarkable ability to enhance the measurement sensitivity beyond the standard quantum limit [4, 5]. This enhancement is particularly critical in sensing applications [6, 7], such as the search for elusive dark matter particles [8] and the observation of gravitational waves [9, 10]. In addition, these nonclassical squeezed states serve as essential resources to generate Gottesman-Kitaev-Preskill states [11, 12], squeezed cat states [13, 14], and squeezed Fock states [15] for quantum error correction protocols [16–19].

Over the past few decades, the generation and manipulation of squeezed states have been successfully demonstrated on a variety of physical platforms [20], including optical and microwave photons [21–28], as well as mechanical and acoustic phonons [29–33]. The underlying mechanism for generating these nonclassical states generally involves engineering a nonlinear interaction within these bosons. The pursuit of a large squeezing typically necessitates a strong nonlinearity, which, however, inevitably introduces additional decoherence and limits the accessibility of the large Hilbert space of an oscillator with a linear displacement drive.

In the realm of quantum optics with superconducting microwave circuits [34], Kerr nonlinearity can be achieved using Josephson junctions, which are essential elements for developing parametric amplifiers [35, 36], generating itinerant squeezed microwave fields [21, 27], and realizing superconducting qubits [37]. By coupling to a strong nonlinear superconducting qubit, a harmonic oscillator in the single-photon

Kerr regime has been demonstrated to realize the collapse and revival of coherent states [38] and to autonomously generate microwave Fock states [39, 40]. In addition, the use of weak Kerr nonlinearities has recently been proposed for manipulating photon-blockaded states [41, 42], with the operation speed enhanced by a large displacement. A similar idea was also demonstrated to implement fast conditional operations [26, 43]. However, despite these theoretical and experimental advancements, demonstrating the fast generation of large squeezed states with a weak Kerr nonlinear oscillator remains a formidable experimental challenge.

In this work, we experimentally demonstrate the generation and amplification of squeezed states in a superconducting microwave cavity with weak Kerr nonlinearity. By subtly engineering an off-resonant microwave drive on the Kerr oscillator, we experimentally observe the cyclic dynamics of the squeezing evolution of Fock states in a displaced frame, without state collapse during the evolution. Intriguingly, the residual photon-blockade interactions are effectively eliminated at the final moment of each cycle, ultimately demonstrating the cyclic squeezing amplification for various Fock states  $|N\rangle$  with  $N$  up to 6 in the cavity. Additionally, we employ the Trotterization technique to realize quantum squeezing amplification by alternately displacing the Kerr oscillator, achieving a maximum squeezing degree of 14.6 dB, which, to our knowledge, is the largest squeezing value for microwave photonic states within the cavity. This ingenious technique offers an efficient approach for realizing displacement-enhanced squeezing operations to generate large squeezed states.

A linear harmonic oscillator has a quadratic potential well, which can be quantized into discrete and equally spaced energy levels, as depicted in Fig. 1(a). The oscillator would induce a self-Kerr nonlinearity when coupling to a nonlin-

ear superconducting qubit in circuit quantum electrodynamics [37]. This nonlinear Kerr oscillator has slightly unequally spaced energy levels with the Hamiltonian expressed as  $H_K = -\frac{K}{2}a^{\dagger 2}a^2$  (assuming  $\hbar = 1$ ) in the rotating frame of the oscillator frequency  $\omega_c$ . Here,  $a(a^\dagger)$  is the annihilation (creation) operator, and  $K$  is the strength of the Kerr nonlinearity of the oscillator. Under this Kerr Hamiltonian, a coherent state will first evolve into a slightly crooked squeezed state and then into a complete phase collapse state [38], as indicated in Fig. 1(b).

To avoid the state collapse and further improve the squeezing degree, we engineer an off-resonant microwave drive on the Kerr oscillator with a drive frequency of  $\omega_d$ , resulting in a driven Kerr oscillator

$$H_d = \Delta_d a^\dagger a - \frac{K}{2} a^{\dagger 2} a^2 + \Omega_d (a + a^\dagger), \quad (1)$$

where  $\Delta_d = \omega_c - \omega_d$  represents the frequency detuning between the oscillator and the drive, and  $\Omega_d$  is the strength of the drive (ignoring the drive phase for simplicity without any loss of generality). This Hamiltonian represents the well-known prototypical model of a quantum Duffing oscillator, exhibiting nonequilibrium phase transition dynamics [44] and nonclassical Wigner negativity [45].

By moving into a displaced frame with a unitary operation of  $D(\beta) = \exp(\beta a^\dagger - \beta^* a)$ , the aforementioned driven Kerr Hamiltonian can be transformed into

$$H_\beta = \Delta' a^\dagger a - \frac{K}{2} a^{\dagger 2} a^2 - \frac{K}{2} (\beta^2 a^{\dagger 2} + \beta^{*2} a^2) - K\beta a^\dagger (a^\dagger a - r) + \text{H.C.} \quad (2)$$

with  $\Delta' = \Delta_d - 2K|\beta|^2$  and  $r = \Delta_d/K + \Omega_d/K\beta - |\beta|^2$  representing the photon-blockade parameter. The first line of the above equation corresponds to the Hamiltonian of a Kerr parametric oscillator, which promises potential applications in quantum computation [46–49], quantum metrology [50], quantum phase transition [51, 52], and quantum tunneling [53, 54].

By properly engineering the detuned drive on the Kerr oscillator, we find that a coherent state no longer collapses during the evolution, as shown in Fig. 1(c). Intriguingly, the coherent state undergoes a cyclic evolution, achieving quantum squeezing amplification at the final moment of each cycle. At this moment, the photon-blockade term is effectively eliminated, resulting in a Kerr parametric oscillator. The displacement-enhanced squeezing can be intuitively understood with the squeezing rate amplified by a factor of  $\beta^2$ , as indicated by the two-photon squeezing term shown in Eq. (2). To find the optimal parameters of the drive frequency detuning and amplitude, we have performed numerical simulations to evaluate the fidelity between the evolved squeezed state and an ideal squeezed state  $|\xi\rangle = S(\xi)|0\rangle$ , where  $S(\xi) = \exp(\frac{\xi^*}{2}a^2 - \frac{\xi}{2}a^{\dagger 2})$  represents a squeezing operator. Here  $\xi$  is a complex number of the squeezing parameter and  $20 \log_{10}(|\xi|)$  defines the squeezing level or squeezing

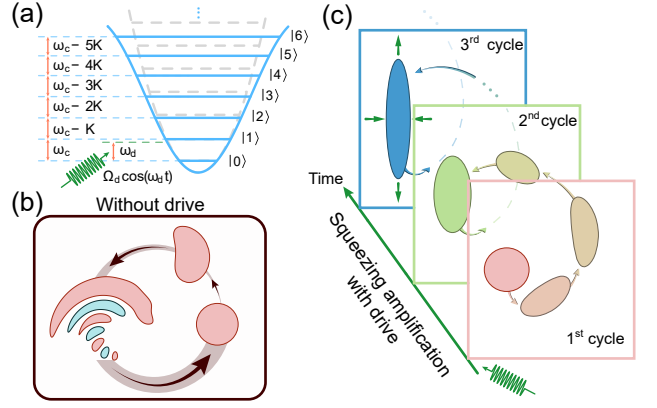


FIG. 1: Schematic illustration for achieving quantum squeezing amplification with a Kerr nonlinear oscillator. **(a)** Energy level diagram of a linear harmonic oscillator (gray dashed lines) and a Kerr nonlinear oscillator (solid blue lines) with an engineered detuned drive of frequency  $\omega_d$  and amplitude  $\Omega_d$  (green wavy line). **(b)** The quantum evolution of a coherent state represented with Wigner functions in phase space, exhibiting squeezing and collapse without any drives on the Kerr oscillator. **(c)** The quantum evolution of a coherent state to realize cyclic squeezing amplification with an engineered detuned drive on the Kerr oscillator. The coherent state undergoes a cyclic evolution in the phase space and becomes a squeezed state at the final moment of each cycle, where the squeezing degree gradually increases with the number of cycles.

degree in dB. The details of the numerical simulation results are presented in the Supplementary Information [55].

In our experiment, we realize a Kerr nonlinear oscillator by dispersively coupling a high-quality superconducting microwave cavity (resonance frequency of  $\omega_c/2\pi = 6.60$  GHz) to an ancillary superconducting qubit (transition frequency of  $\omega_q/2\pi = 5.28$  GHz). The cavity mode has a weak Kerr nonlinearity of  $K/2\pi = 5.83$  kHz ( $K/\omega_c < 10^{-6}$ ) and a single-photon lifetime of  $395 \mu\text{s}$  (corresponding to a decay rate  $\kappa_c/2\pi = 0.40$  kHz), serving as the storage cavity for storing and manipulating the multiphoton squeezed states. The ancillary qubit mode, with an energy relaxation time of about  $38 \mu\text{s}$  and a pure dephasing time of  $146 \mu\text{s}$ , is utilized for characterizing the generated squeezed states in the storage cavity. Detailed information regarding the device parameters and experimental setup is provided in the Supplementary Information [55]. Note that, our displacement-enhanced squeezing method is also applicable even with an ultra-weak Kerr nonlinearity  $K < \kappa_c$  (see Supplementary Information [55]).

The experimental sequence is shown in Fig. 2(a), where the initial cavity vacuum state is first transformed into a displaced frame using a displacement operation  $D(\beta)$ , then evolves under the detuned driven Kerr Hamiltonian, and finally reverts to the original frame via a reverse displacement operation  $D(-\beta)$ . To achieve a larger squeezing degree, we choose an optimal displacement amplitude  $\beta = 2$ , and drive frequency detuning  $\Delta_d/2\pi = 56$  kHz and amplitude  $\Omega_d/2\pi = 2.01$  MHz, as determined from numerical simulations (see Supplementary Information [55]). At the end of

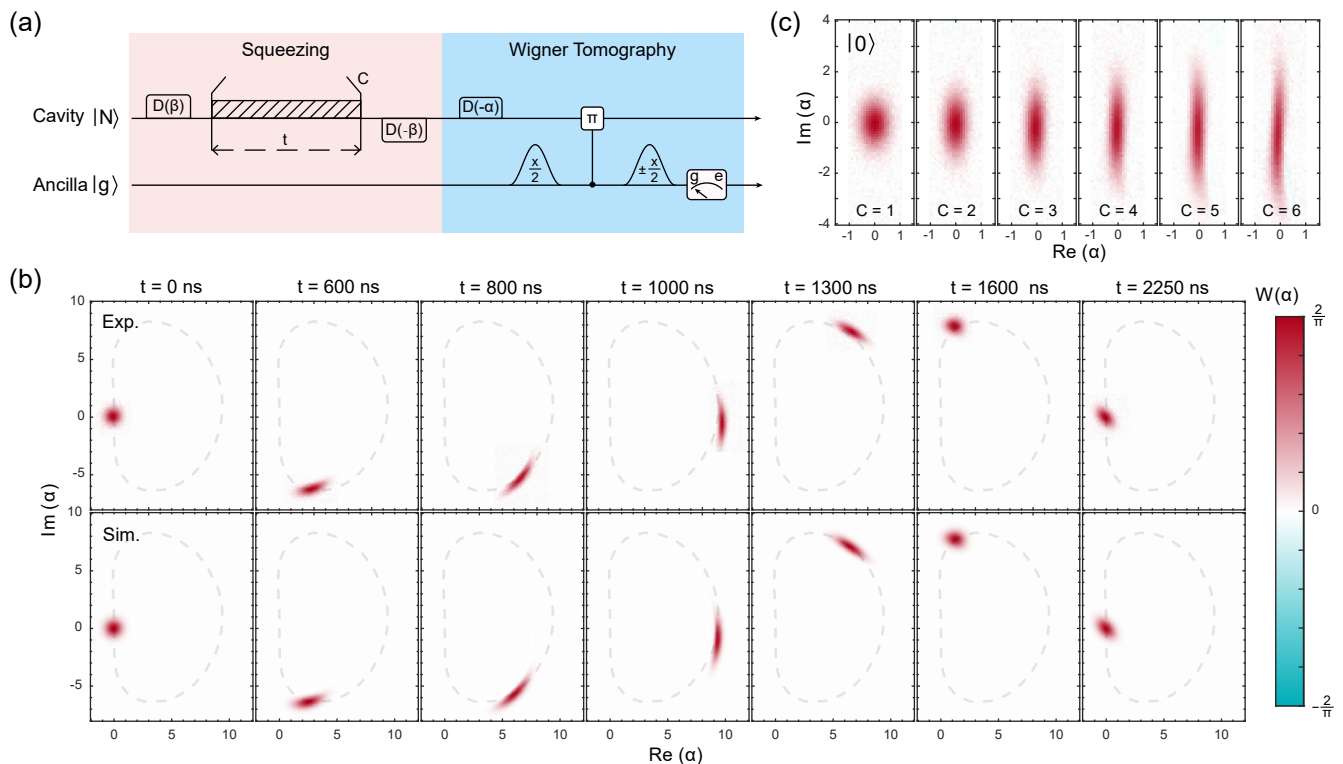


FIG. 2: Cyclic squeezing evolution with a detuned drive on the Kerr nonlinear oscillator for generating squeezed vacuum states. **(a)** Experimental sequence for cyclic squeezing evolution and characterization with Wigner tomography. **(b)** Experimentally measured (top row) and numerically simulated (bottom row) Wigner function snapshots for the cyclic squeezing evolution of a vacuum state  $|N = 0\rangle$  in the first cycle ( $C=1$ ), showcasing that the quantum state no longer collapses during the evolution and evolves into a squeezed state at the final moment of each cycle. **(c)** Experimentally measured Wigner functions of the generated squeezed vacuum states at the final moment of the first 6 evolutionary cycles, obviously indicating that the squeezing is enhanced as the number of cycles increases.

the sequence, we employ Wigner tomography to characterize the cavity states. During the first evolution cycle with a period of 2250 ns, we measure the Wigner functions of the cavity states at various moments, which are in good agreement with numerical simulations, as indicated in Fig. 2(b). The measurement results reveal that the coherent state rotates without collapsing in phase space under the detuned driven Kerr Hamiltonian, and is compressed into an elliptical structure in phase space at the end of each evolution cycle, indicating the successful generation of squeezed states. We displace the compressed coherent state to the origin in phase space, perform a virtual phase rotation operation to eliminate the rotation angle [55], and measure the Wigner functions of the generated squeezed states at the final moment of different cycles. The experimental results displayed in Fig. 2(c), clearly show that as the number of cycles increases, the cavity state is gradually compressed in one direction and stretched in the orthogonal direction. This structural feature indicates that the squeezing level of the cavity state is progressively amplified as increasing cycles, demonstrating the effectiveness of the displacement-enhanced squeezing approach.

Additionally, the displacement-enhanced squeezing approach is not limited to vacuum states but is also applicable

to multiphoton Fock states as the initial cavity state. The experimental sequence is similar to that in Fig. 2(a) with only replacing the initial vacuum state  $|0\rangle$  with the multiphoton Fock state  $|N\rangle$ , which is generated using numerically optimized pulses assisted by the ancillary qubit [56]. In Fig. 3(a-c), we present the measured Wigner functions of the generated squeezed Fock states for various evolution cycles. The experimental results indicate that as the number of cycles increases, the multiphoton Fock states are progressively squeezed in one quadrature, exhibiting enhanced squeezing levels.

By performing a two-dimensional (2D) fit to the measured Wigner functions of both the squeezed Fock states and vacuum states, we extract the squeezing levels of these nonclassical states as a function of the number of evolution cycles, as depicted in Fig. 3(d). We perform a linear fit to the squeezing levels of vacuum states within the linear region, achieving an average increase in squeezing level of 1.92 dB per cycle. These experimental results demonstrate that multiphoton Fock states can also be squeezed, with the squeezing parameters amplified through displacement-enhanced squeezing operations. The generated squeezed Fock states, with a large squeezing level and photon number, could potentially achieve higher sensitivities than either squeezed vacuum states or

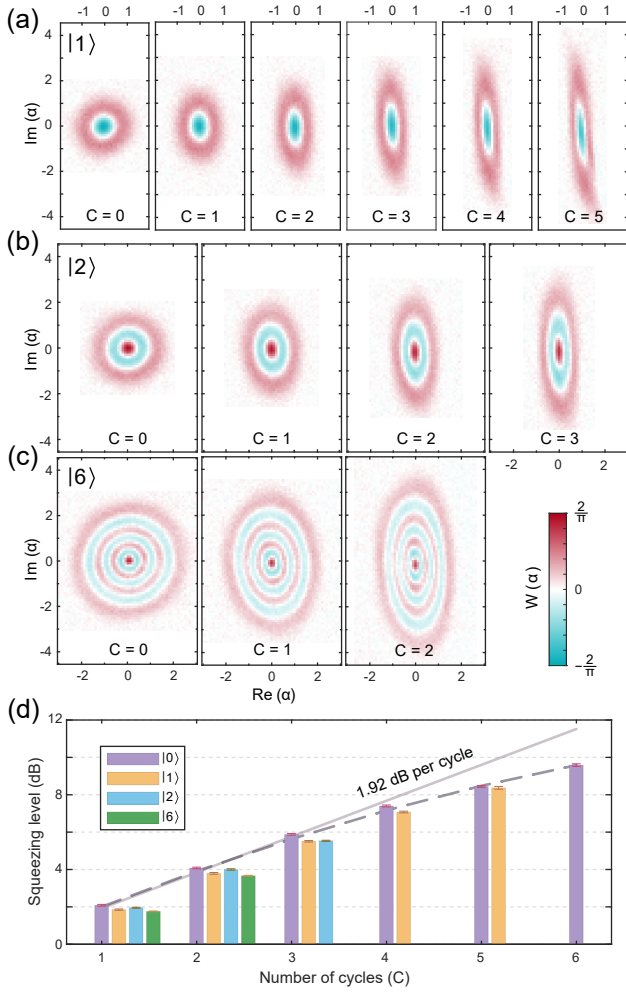


FIG. 3: Generation of squeezed Fock states with a detuned drive on the Kerr nonlinear oscillator. **(a-c)** Experimentally measured Wigner functions of the generated squeezed Fock states  $|N\rangle$  for various evolutionary cycles with  $N = 1$  (a), 2 (b), and 6 (c), respectively. **(d)** The extracted squeezing levels obtained from 2D fits to the measured Wigner functions of the generated squeezed Fock states as a function of the number of cycles. Error bars are the estimated 95% confidence intervals of the fittings. The solid line is a linear fit to the squeezing level for vacuum states in linear region, showing an average addition in squeezing level of 1.92 dB per cycle. The dashed line represents squeezing levels for vacuum states from numerical simulation.

multiphoton-number Fock states alone, offering significant advantages in quantum-enhanced precision metrology.

It is noted that the squeezing levels are gradually saturated as increasing the evolution cycles, which is primarily attributed to the remaining Kerr nonlinearity and the residual photon-blockade term in the Hamiltonian of Eq. (2). Here, we propose to utilize the Trotterization technique [57] to eliminate the photon-blockade Hamiltonian to enhance the squeezing levels further. The key point of this approach lies in the addition of the driven Kerr Hamiltonian in two opposite displacement frames,  $H_\beta$  and  $H_{-\beta}$ , which could completely eliminate the photon-blockade term, resulting in a Kerr para-

metric oscillator Hamiltonian:

$$H_{\text{KPO}} = \frac{H_\beta + H_{-\beta}}{2} = \Delta' a^\dagger a - \frac{K}{2} a^{\dagger 2} a^2 - \frac{K}{2} (\beta^2 a^{\dagger 2} + \beta^{*2} a^2). \quad (3)$$

Intuitively, by alternating the phases of the displacement frame, we can effectively eliminate the undesired photon-blockade term while preserving the two-photon squeezing term for achieving fast squeezing operation. Based on the Trotterization formula, the time evolution of the Kerr parametric oscillator Hamiltonian can be expressed as

$$e^{-iH_{\text{KPO}}\delta t} = e^{-iH_{-\beta}\delta t/2} e^{-iH_\beta\delta t/2} + \mathcal{O}[(\delta t)^2], \quad (4)$$

in a discretized evolutionary time step  $\delta t$  with Trotter errors suppressed to an order of  $\mathcal{O}[(\delta t)^2]$ . By increasing the displacement amplitude  $\beta$ , the two-photon squeezing term would dominate in the Kerr parametric oscillator Hamiltonian of Eq. (3) for achieving large squeezed states. Note that in this scenario, the detuned drive during the Kerr evolution is unnecessary, so we set  $\Omega_d = 0$  to restrict the average photon number of the intermediate states and engineer the frequency detuning to mitigate the Kerr-induced phases on the squeezed states [55].

The experimental sequence to demonstrate the quantum squeezing amplification with the Trotterization method is shown in Fig. 4(a). In this sequence, we alternately transform the Kerr oscillator into different displacement frames with opposite phases. This is similar to an echoed displaced Kerr evolution that would average away the undesired photon-blockade term. To evaluate the squeezing performance of the generated squeezed states, we measure one-dimensional (1D) Wigner function cuts along the real axis ( $\text{Im}(\alpha) = 0$ ) and the imaginary axis ( $\text{Re}(\alpha) = 0$ ), respectively, with the experimental results shown in Fig. 4(b). As increasing the Trotter steps, the linewidth of one trace is compressed below  $1/2$ , while the other one is expanded beyond  $1/2$ , indicating an effective squeezing of the quantum state. From a global fit to both traces, we extract the squeezing parameters  $|\xi|$  of the generated squeezed states as a function of the number of Trotter steps for various displacement amplitudes  $|\beta|$ , with the experimental results shown in Fig. 4(c).

The experimental results reveal that as the number of Trotter steps increases, the squeezing level is amplified towards a large squeezed state. The eventual saturation in squeezing levels is attributed to Kerr nonlinearity, verified by numerical simulations. By performing a linear fit to the experimental data within the linear region, we extract the squeezing rate as a function of  $|\beta|^2$ , as shown in the inset of Fig. 4(c). As the displacement amplitude  $|\beta|$  increases, the squeezing rate is enhanced accordingly, but deviates from the ideal relationship  $K\beta^2$ . This deviation is primarily due to the neglect of Kerr evolution during the displacement operation and the influence of higher-order Kerr nonlinearities. When these aspects are taken into account, the numerical simulation results align well with the experimental data.

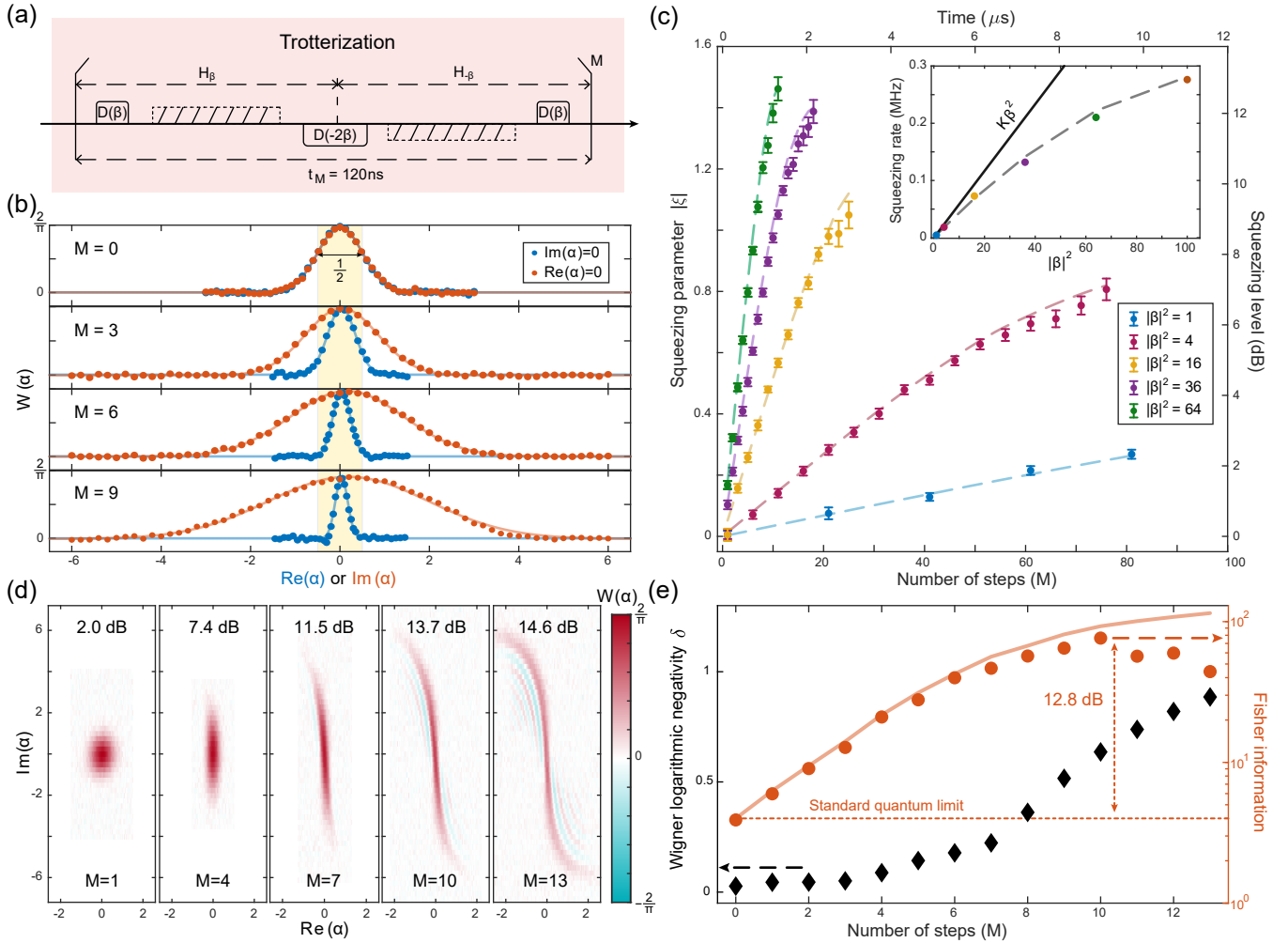


FIG. 4: Quantum squeezing amplification with Trotterization technique. (a) Experimental sequence of the Trotter steps for realizing the squeezing amplification. (b) Measured 1D Wigner function cuts along the real axis (blue symbols) and the imaginary axis (red symbols) of the generated squeezed states for various Trotter steps. Solid lines are a global fit to these two traces at each Trotter step. (c) Experimentally extracted (symbols) and numerically simulated (dashed lines) squeezing parameters as a function of the number of Trotter steps (bottom axis) or the evolutionary time (top axis) for various displacement amplitudes  $|\beta|^2$ . The inset exhibits the extracted squeezing rates as a function of the displacement amplitude  $|\beta|^2$ , which agree well with the simulation results (dashed line). Solid line represents the ideal squeezing rate of  $K\beta^2$ . (d) Measured 2D Wigner functions of the generated squeezed states for various Trotter steps with  $|\beta|^2 = 100$ . (e) Extracted Wigner logarithmic negativities and FI for the generated squeezed states shown in (d). A maximum metrological gain of 12.8 dB is achieved for the extracted FI over the standard quantum limit. Solid line corresponds to the FI for ideal squeezed states.

Furthermore, we have measured the 2D Wigner functions of the generated states at various Trotter steps, as shown in Fig. 4(d). The 2D Wigner fitting results demonstrate a maximum squeezing degree of 14.6 dB, which is larger than previous demonstrations of intracavity squeezing [24–26, 28]. Despite the gradual twist and stretch of the squeezed states in phase space due to Kerr nonlinearity, these states continue to exhibit large nonclassicality characterized by the Wigner logarithmic negativity  $\delta = \log_2(\int d\alpha |W(\alpha)|)$  [58]. The extracted Wigner logarithmic negativities as a function of the number of Trotter steps are presented in Fig. 4(e), highlighting the substantial nonclassicality of the generated quantum states. Additionally, these nonclassical states exhibit large Fisher information

(FI), which quantifies the maximum information that can be extracted about a parameter from the quantum state. The FI is calculated using the formula  $\int dx (\partial_x \ln P(x))^2 P(x)$  to estimate the measurement sensitivity of small displacement along the position quadrature, where  $P(x) = \int dp W(\alpha = x + ip)$  represents the position probability distribution [26]. The calculated FI as a function of the number of Trotter steps is also presented in Fig. 4(e). We observe that as the number of Trotter steps increases, the FI is greatly enhanced, demonstrating the large metrological advantage of these nonclassical states in surpassing the standard quantum limit.

In conclusion, we have experimentally demonstrated displacement-enhanced quantum squeezing amplification by

off-resonantly driving a weak Kerr nonlinear oscillator within a superconducting microwave cavity, leveraging the Trotterization technique. This method distinguishes itself from previous displacement-enhanced operations [26, 43] by eliminating decoherence errors induced by the ancillary qubit during the evolution. Our approach ultimately generates nonclassical microwave photonic states with a maximum squeezing degree of 14.6 dB over quasiclassical coherent states. The squeezing degree can be further enhanced by engineering a weaker Kerr nonlinearity and a larger displacement amplitude [55]. These large squeezed states are demonstrated to exhibit large Fisher information, promising potential applications in quantum-enhanced metrology [50]. Furthermore, our approach provides a hardware-efficient way to engineer strong two-photon squeezing operations, which is beneficial for quantum information processing with Kerr cat qubits [46–48], bosonic quantum chemistry simulations [59], and topological phase transitions [51, 52], as well as for reducing decoherence of quantum systems [14, 60, 61]. A recent notable advancement in quantum squeezing with acoustic wave resonators [32] suggests the potential for easily adapting our approach to achieve even larger squeezing with microwave phonons, photons, or magnons in qubit-oscillator systems [29, 62–64].

This work was supported by the Guangdong Basic and Applied Basic Research Foundation (Grant No. 2024B1515020013), the National Natural Science Foundation of China (Grants No. 12422416, No. 12274198), the Shenzhen Science and Technology Program (Grant No. RCYX20210706092103021), the Guangdong Provincial Key Laboratory (Grant No. 2019B121203002), the Shenzhen-Hong Kong cooperation zone for technology and innovation (Contract No. HZQB-KCZYB-2020050), the Innovation Program for Quantum Science and Technology (Grant No. 2021ZD0301703).

---

\* These authors contributed equally to this work.

† Electronic address: [xuyuan@iqasz.cn](mailto:xuyuan@iqasz.cn)

- [1] S. L. Braunstein and P. van Loock, “Quantum information with continuous variables,” *Rev. Mod. Phys.* **77**, 513 (2005).
- [2] U. Andersen, G. Leuchs, and C. Silberhorn, “Continuous-variable quantum information processing,” *Laser & Photon. Rev.* **4**, 337 (2010).
- [3] H. P. Yuen, “Two-photon coherent states of the radiation field,” *Phys. Rev. A* **13**, 2226 (1976).
- [4] C. M. Caves, “Quantum-mechanical noise in an interferometer,” *Phys. Rev. D* **23**, 1693 (1981).
- [5] D. F. Walls, “Squeezed states of light,” *Nature* **306**, 141 (1983).
- [6] R. Schnabel, “Squeezed states of light and their applications in laser interferometers,” *Phys. Rep.* **684**, 1 (2017).
- [7] B. J. Lawrie, P. D. Lett, A. M. Marino, and R. C. Pooser, “Quantum Sensing with Squeezed Light,” *ACS Photonics* **6**, 1307 (2019).
- [8] K. M. Backes, D. A. Palken, S. A. Kenany, B. M. Brubaker, S. B. Cahn, *et al.*, “A quantum enhanced search for dark matter axions,” *Nature* **590**, 238 (2021).
- [9] J. Abadie, B. P. Abbott, R. Abbott, T. D. Abbott, M. Abernathy, *et al.*, “A gravitational wave observatory operating beyond the quantum shot-noise limit,” *Nat. Phys.* **7**, 962 (2011).
- [10] M. Tse, H. Yu, N. Kijbunchoo, A. Fernandez-Galiana, P. Dupej, *et al.*, “Quantum-enhanced advanced LIGO detectors in the era of gravitational-wave astronomy,” *Phys. Rev. Lett.* **123**, 231107 (2019).
- [11] C. Flühmann, T. L. Nguyen, M. Marinelli, V. Negnevitsky, K. Mehta, and J. P. Home, “Encoding a qubit in a trapped-ion mechanical oscillator,” *Nature* **566**, 513 (2019).
- [12] J. Hastrup, K. Park, J. B. Brask, R. Filip, and U. L. Andersen, “Measurement-free preparation of grid states,” *npj Quantum Inf.* **7**, 17 (2021).
- [13] H.-Y. Lo, D. Kienzler, L. de Clercq, M. Marinelli, V. Negnevitsky, B. C. Keitch, and J. P. Home, “Spin–motion entanglement and state diagnosis with squeezed oscillator wavepackets,” *Nature* **521**, 336 (2015).
- [14] X. Pan, J. Schwinger, N.-N. Huang, P. Song, W. Chua, F. Hanamura, A. Joshi, F. Valadares, R. Filip, and Y. Y. Gao, “Protecting the Quantum Interference of Cat States by Phase-Space Compression,” *Phys. Rev. X* **13**, 021004 (2023).
- [15] D. Kienzler, H.-Y. Lo, V. Negnevitsky, C. Flühmann, M. Marinelli, and J. P. Home, “Quantum harmonic oscillator state control in a squeezed Fock basis,” *Phys. Rev. Lett.* **119**, 033602 (2017).
- [16] P. Campagne-Ibarcq, A. Eickbusch, S. Touzard, E. Zalys-Geller, N. E. Frattini, V. V. Sivak, P. Reinhold, S. Puri, S. Shankar, R. J. Schoelkopf, L. Frunzio, M. Mirrahimi, and M. H. Devoret, “Quantum error correction of a qubit encoded in grid states of an oscillator,” *Nature* **584**, 368 (2020).
- [17] D. S. Schlegel, F. Minganti, and V. Savona, “Quantum error correction using squeezed Schrödinger cat states,” *Phys. Rev. A* **106**, 022431 (2022).
- [18] Q. Xu, G. Zheng, Y.-X. Wang, P. Zoller, A. A. Clerk, and L. Jiang, “Autonomous quantum error correction and fault-tolerant quantum computation with squeezed cat qubits,” *npj Quantum Inf.* **9**, 78 (2023).
- [19] S. B. Korolev, E. N. Bashmakova, and T. Yu. Golubeva, “Error correction using squeezed Fock states,” *Quantum Inf. Process.* **23**, 354 (2024).
- [20] U. L. Andersen, T. Gehring, C. Marquardt, and G. Leuchs, “30 years of squeezed light generation,” *Phys. Scr.* **91**, 053001 (2016).
- [21] B. Yurke, P. G. Kaminsky, R. E. Miller, E. A. Whittaker, A. D. Smith, A. H. Silver, and R. W. Simon, “Observation of 4.2-K equilibrium-noise squeezing via a Josephson-parametric amplifier,” *Phys. Rev. Lett.* **60**, 764 (1988).
- [22] H. Vahlbruch, M. Mehmet, S. Chelkowski, B. Hage, A. Franzen, N. Lastzka, S. Goßler, K. Danzmann, and R. Schnabel, “Observation of Squeezed Light with 10-dB Quantum-Noise Reduction,” *Phys. Rev. Lett.* **100**, 033602 (2008).
- [23] A. H. Safavi-Naeini, S. Gröblacher, J. T. Hill, J. Chan, M. Aspelmeyer, and O. Painter, “Squeezed light from a silicon micromechanical resonator,” *Nature* **500**, 185 (2013).
- [24] W. Wang, L. Hu, Y. Xu, K. Liu, Y. Ma, S.-B. Zheng, R. Vijay, Y. P. Song, L.-M. Duan, and L. Sun, “Converting Quasiclassical States into Arbitrary Fock State Superpositions in a Superconducting Circuit,” *Phys. Rev. Lett.* **118**, 223604 (2017).
- [25] R. Dassonneville, R. Assouly, T. Peronnin, A. Clerk, A. Bienfait, and B. Huard, “Dissipative Stabilization of Squeezing Beyond 3 dB in a Microwave Mode,” *PRX Quantum* **2**, 020323 (2021).
- [26] A. Eickbusch, V. Sivak, A. Z. Ding, S. S. Elder, S. R. Jha, J. Venkatraman, B. Royer, S. M. Girvin, R. J. Schoelkopf, and M. H. Devoret, “Fast universal control of an oscillator

- with weak dispersive coupling to a qubit,” *Nat. Phys.* **18**, 1464 (2022).
- [27] J. Y. Qiu, A. Grimsmo, K. Peng, B. Kannan, B. Lienhard, Y. Sung, P. Krantz, V. Bolkhovsky, G. Calusine, D. Kim, A. Melville, B. M. Niedzielski, J. Yoder, M. E. Schwartz, T. P. Orlando, I. Siddiqi, S. Gustavsson, K. P. O’Brien, and W. D. Oliver, “Broadband squeezed microwaves and amplification with a Josephson travelling-wave parametric amplifier,” *Nat. Phys.* **19**, 706 (2023).
- [28] A. M. Eriksson, T. S epulcre, M. Kervinen, T. Hillmann, M. Kudra, S. Dupouy, Y. Lu, M. Khanahmadi, J. Yang, C. Castillo-Moreno, P. Delsing, and S. Gasparinetti, “Universal control of a bosonic mode via drive-activated native cubic interactions,” *Nat. Commun.* **15**, 2512 (2024).
- [29] E. E. Wollman, C. U. Lei, A. J. Weinstein, J. Suh, A. Kronwald, F. Marquardt, A. A. Clerk, and K. C. Schwab, “Quantum squeezing of motion in a mechanical resonator,” *Science* **349**, 952 (2015).
- [30] X. Ma, J. J. Viennot, S. Kotler, J. D. Teufel, and K. W. Lehnert, “Non-classical energy squeezing of a macroscopic mechanical oscillator,” *Nat. Phys.* **17**, 322 (2021).
- [31] A. Youssefi, S. Kono, M. Chegnizadeh, and T. J. Kippenberg, “A squeezed mechanical oscillator with millisecond quantum decoherence,” *Nat. Phys.* **19**, 1697 (2023).
- [32] S. Marti, U. von L upke, O. Joshi, Y. Yang, M. Bild, A. Omanen, Y. Chu, and M. Fadel, “Quantum squeezing in a nonlinear mechanical oscillator,” *Nat. Phys.* **20**, 1448 (2024).
- [33] V. G. Matsos, C. H. Valahu, T. Navickas, A. D. Rao, M. J. Millican, X. C. Kolesnikow, M. J. Biercuk, and T. R. Tan, “Robust and Deterministic Preparation of Bosonic Logical States in a Trapped Ion,” *Phys. Rev. Lett.* **133**, 050602 (2024).
- [34] X. Gu, A. F. Kockum, A. Miranowicz, Y.-x. Liu, and F. Nori, “Microwave photonics with superconducting quantum circuits,” *Phys. Rep.* **718–719**, 1 (2017).
- [35] N. Bergeal, F. Schackert, M. Metcalfe, R. Vijay, V. E. Manucharyan, L. Frunzio, D. E. Prober, R. J. Schoelkopf, S. M. Girvin, and M. H. Devoret, “Phase-preserving amplification near the quantum limit with a Josephson ring modulator,” *Nature* **465**, 64 (2010).
- [36] C. Macklin, K. O’Brien, D. Hover, M. E. Schwartz, V. Bolkhovsky, X. Zhang, W. D. Oliver, and I. Siddiqi, “A near-quantum-limited Josephson traveling-wave parametric amplifier,” *Science* **350**, 307 (2015).
- [37] A. Blais, A. L. Grimsmo, S. M. Girvin, and A. Wallraff, “Circuit quantum electrodynamics,” *Rev. Mod. Phys.* **93**, 025005 (2021).
- [38] G. Kirchmair, B. Vlastakis, Z. Leghtas, S. E. Nigg, H. Paik, E. Ginossar, M. Mirrahimi, L. Frunzio, S. M. Girvin, and R. J. Schoelkopf, “Observation of quantum state collapse and revival due to the single-photon Kerr effect,” *Nature* **495**, 205 (2013).
- [39] E. T. Holland, B. Vlastakis, R. W. Heeres, M. J. Reagor, U. Vool, Z. Leghtas, L. Frunzio, G. Kirchmair, M. H. Devoret, M. Mirrahimi, and R. J. Schoelkopf, “Single-Photon-Resolved Cross-Kerr Interaction for Autonomous Stabilization of Photon-Number States,” *Phys. Rev. Lett.* **115**, 180501 (2015).
- [40] S. Li, Z. Ni, L. Zhang, Y. Cai, J. Mai, S. Wen, P. Zheng, X. Deng, S. Liu, Y. Xu, and D. Yu, “Autonomous Stabilization of Fock States in an Oscillator against Multiphoton Losses,” *Phys. Rev. Lett.* **132**, 203602 (2024).
- [41] A. Lingenfelter, D. Roberts, and A. A. Clerk, “Unconditional Fock state generation using arbitrarily weak photonic nonlinearities,” *Sci. Adv.* **7**, eabj1916 (2021).
- [42] M. Yuan, A. Seif, A. Lingenfelter, D. I. Schuster, A. A. Clerk, and L. Jiang, “Universal Control in Bosonic Systems with Weak Kerr Nonlinearities,” *arXiv: 2312.15783* (2023).
- [43] A. A. Diringier, E. Blumenthal, A. Grinberg, L. Jiang, and S. Hacoheh-Gourgy, “Conditional-not Displacement: Fast Multioscillator Control with a Single Qubit,” *Phys. Rev. X* **14**, 011055 (2024).
- [44] Q.-M. Chen, M. Fischer, Y. Nojiri, M. Renger, E. Xie, M. Partanen, S. Pogorzalek, K. G. Fedorov, A. Marx, F. Deppe, and R. Gross, “Quantum behavior of the Duffing oscillator at the dissipative phase transition,” *Nat. Commun.* **14**, 2896 (2023).
- [45] C. A. Rosiek, M. Rossi, A. Schliesser, and A. S. S orensen, “Quadrature Squeezing Enhances Wigner Negativity in a Mechanical Duffing Oscillator,” *PRX Quantum* **5**, 030312 (2024).
- [46] H. Goto, “Bifurcation-based adiabatic quantum computation with a nonlinear oscillator network,” *Sci. Rep.* **6**, 21686 (2016).
- [47] S. Puri, S. Boutin, and A. Blais, “Engineering the quantum states of light in a Kerr-nonlinear resonator by two-photon driving,” *npj Quantum Inf.* **3**, 18 (2017).
- [48] A. Grimm, N. E. Frattini, S. Puri, S. O. Mundhada, S. Touzard, M. Mirrahimi, S. M. Girvin, S. Shankar, and M. H. Devoret, “Stabilization and operation of a Kerr-cat qubit,” *Nature* **584**, 205 (2020).
- [49] N. E. Frattini, R. G. Corti nas, J. Venkatraman, X. Xiao, Q. Su, C. U. Lei, B. J. Chapman, V. R. Joshi, S. M. Girvin, R. J. Schoelkopf, S. Puri, and M. H. Devoret, “Observation of pairwise level degeneracies and the quantum regime of the arrhenius law in a double-well parametric oscillator,” *Phys. Rev. X* **14**, 031040 (2024).
- [50] J. Guo, Q. He, and M. Fadel, “Quantum metrology with a squeezed Kerr oscillator,” *Phys. Rev. A* **109**, 052604 (2024).
- [51] J. Ch avez-Carlos, T. L. M. Lezama, R. G. Corti nas, J. Venkatraman, M. H. Devoret, V. S. Batista, F. P erez-Bernal, and L. F. Santos, “Spectral kissing and its dynamical consequences in the squeeze-driven Kerr oscillator,” *npj Quantum Inf.* **9**, 76 (2023).
- [52] H.-L. Zhang, J.-H. L u, K. Chen, X.-J. Yu, F. Wu, Z.-B. Yang, and S.-B. Zheng, “Critical quantum geometric tensors of parametrically-driven nonlinear resonators,” *Opt. Express* **32**, 22566 (2024).
- [53] M. A. P. Reynoso, D. J. Nader, J. Ch avez-Carlos, B. E. Ordaz-Mendoza, R. G. Corti nas, V. S. Batista, S. Lerma-Hern andez, F. P erez-Bernal, and L. F. Santos, “Quantum tunneling and level crossings in the squeeze-driven Kerr oscillator,” *Phys. Rev. A* **108**, 033709 (2023).
- [54] D. Iyama, T. Kamiya, S. Fujii, H. Mukai, Y. Zhou, T. Nagase, A. Tomonaga, R. Wang, J.-J. Xue, S. Watabe, S. Kwon, and J.-S. Tsai, “Observation and manipulation of quantum interference in a superconducting Kerr parametric oscillator,” *Nat. Commun.* **15**, 86 (2024).
- [55] Supplementary Information .
- [56] R. W. Heeres, P. Reinhold, N. Ofek, L. Frunzio, L. Jiang, M. H. Devoret, and R. J. Schoelkopf, “Implementing a universal gate set on a logical qubit encoded in an oscillator,” *Nat. Commun.* **8**, 94 (2017).
- [57] S. Lloyd, “Universal quantum simulators,” *Science* **273**, 1073 (1996).
- [58] F. Albarelli, M. G. Genoni, M. G. A. Paris, and A. Ferraro, “Resource theory of quantum non-Gaussianity and Wigner negativity,” *Phys. Rev. A* **98**, 052350 (2018).
- [59] R. Dutta, D. G. A. Cabral, N. Lyu, N. P. Vu, Y. Wang, B. Allen, X. Dan, R. G. Corti nas, P. Khazaei, M. Sch afer, A. C. C. D. Albornoz, S. E. Smart, S. Nie, M. H. Devoret, D. A. Mazziotti, P. Narang, C. Wang, J. D. Whitfield, A. K. Wilson, H. P. Hendrickson, D. A. Lidar, F. P erez-Bernal, L. F. Santos, S. Kais, E. Geva, and V. S. Batista, “Simulating Chemistry on Bosonic

- Quantum Devices,” *J. Chem. Theory Comput.* **20**, 6426 (2024).
- [60] K. W. Murch, S. J. Weber, K. M. Beck, E. Ginossar, and I. Siddiqi, “Reduction of the radiative decay of atomic coherence in squeezed vacuum,” *Nature* **499**, 62 (2013).
- [61] H. Le Jeannic, A. Cavaillès, K. Huang, R. Filip, and J. Laurat, “Slowing Quantum Decoherence by Squeezing in Phase Space,” *Phys. Rev. Lett.* **120**, 073603 (2018).
- [62] Y. Tabuchi, S. Ishino, A. Noguchi, T. Ishikawa, R. Yamazaki, K. Usami, and Y. Nakamura, “Coherent coupling between a ferromagnetic magnon and a superconducting qubit,” *Science* **349**, 405 (2015).
- [63] U. von Lüpke, Y. Yang, M. Bild, L. Michaud, M. Fadel, and Y. Chu, “Parity measurement in the strong dispersive regime of circuit quantum acoustodynamics,” *Nat. Phys.* **18**, 794 (2022).
- [64] Y. Liu, S. Singh, K. C. Smith, E. Crane, J. M. Martyn, A. Eickbusch, A. Schuckert, R. D. Li, J. Sinanan-Singh, M. B. Soley, T. Tsunoda, I. L. Chuang, N. Wiebe, and S. M. Girvin, “Hybrid Oscillator-Qubit Quantum Processors: Instruction Set Architectures, Abstract Machine Models, and Applications,” *arXiv:2407.10381* (2024).



TABLE S1: Device parameters of the system.

Parameters	Value
Storage cavity frequency $\omega_c/2\pi$ (GHz)	6.60
Storage cavity Kerr nonlinearity $K/2\pi$ (kHz)	5.83
Storage cavity dispersive shift $\chi_{qc}/2\pi$ (MHz)	1.94
Storage cavity relaxation $T_{1,c}$ ( $\mu$ s)	395
Storage cavity Ramsey coherence $T_{2,c}$ ( $\mu$ s)	595
Storage cavity thermal population	0.1%
Qubit frequency $\omega_q/2\pi$ (GHz)	5.28
Qubit anharmonicity $\eta_q/2\pi$ (MHz)	194.6
Qubit relaxation $T_{1,q}$ ( $\mu$ s)	38
Qubit Ramsey coherence $T_{2,q}$ ( $\mu$ s)	50
Qubit echo coherence $T_{2E,q}$ ( $\mu$ s)	58
Qubit thermal population	1.15%
Readout frequency $\omega_r/2\pi$ (GHz)	8.67
Readout decay rate $\kappa_r/2\pi$ (MHz)	3.8
Readout dispersive shift $\chi_{qr}/2\pi$ (MHz)	2.0

nian expressed as:

$$\begin{aligned}
H/\hbar = & \omega_c a^\dagger a - \frac{K}{2} a^{\dagger 2} a^2 \\
& + \omega_q q^\dagger q - \frac{\eta_q}{2} q^{\dagger 2} q^2 - \chi_{qc} a^\dagger a q^\dagger q \\
& + \omega_r a_r^\dagger a_r - \chi_{qr} a_r^\dagger a_r q^\dagger q,
\end{aligned} \quad (\text{S1})$$

where  $a, q$  and  $a_r$  are the annihilation operators for the storage cavity, superconducting qubit, and readout resonator, respectively;  $\omega_c$ ,  $\omega_q$ , and  $\omega_r$  are their respective resonance frequencies;  $K$  is the Kerr nonlinearity of storage cavity;  $\eta_q$  is the anharmonicity of the qubit; and  $\chi_{qc}$  and  $\chi_{qr}$  are the cross-Kerr interactions between the qubit and the storage cavity and readout resonator, respectively. The measured values of these parameters are summarized and listed in Table S1.

Focusing solely on the storage cavity mode, the above Hamiltonian simplifies to a Kerr nonlinear Hamiltonian  $H_K = \omega_c a^\dagger a - \frac{K}{2} a^{\dagger 2} a^2$  (assuming  $\hbar = 1$ ). Under this Hamiltonian, a coherent state evolves into a slightly squeezed state and then collapses in phase space [9]. By applying an engineered off-resonant microwave drive  $\Omega_d(e^{i\omega_d t} a + e^{-i\omega_d t} a^\dagger)$ , the coherent state undergoes a cyclic squeezing dynamics evolution in phase space without collapse. Here,  $\Omega_d$  and  $\omega_d$  denote the drive strength and frequency, respectively. In the rotating frame of the oscillator frequency  $\omega_c$ , the driven Kerr Hamiltonian is expressed as:

$$H_d = \Delta_d a^\dagger a - \frac{K}{2} a^{\dagger 2} a^2 + \Omega_d (a + a^\dagger), \quad (\text{S2})$$

where  $\Delta_d = \omega_c - \omega_d$  is the frequency detuning between the oscillator and the drive. By appropriately engineering the off-resonant drive, we achieve cyclic squeezing evolution of a coherent state  $|\beta\rangle$ , which is initialized using a displacement operator  $D(\beta) = e^{\beta a^\dagger - \beta^* a}$ .

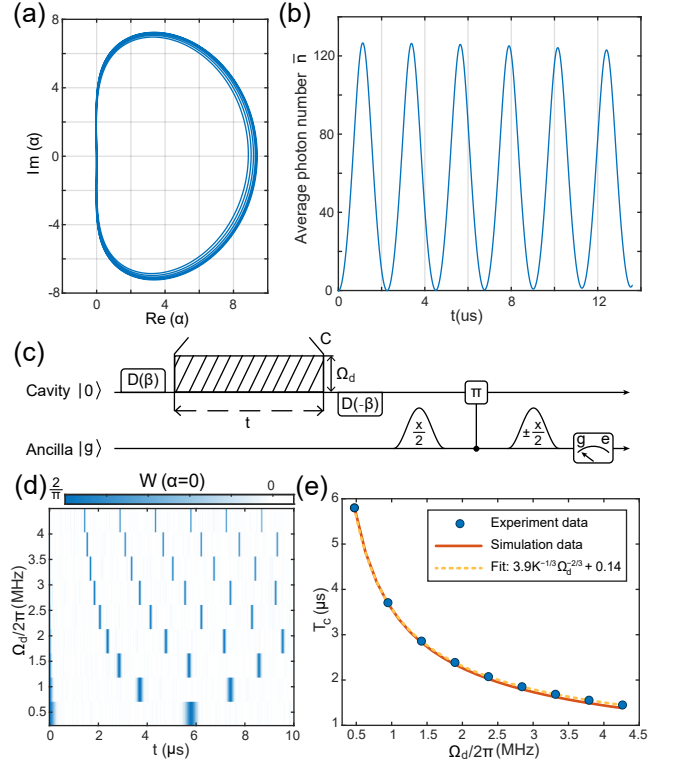


FIG. S2: Cyclic evolution of the driven Kerr nonlinear oscillator. (a) Quantum state trajectories for the first six evolutionary cycles in phase space. (b) Time evolution of the average photon number of the quantum state in the cavity. (c) Experimental sequence for demonstrating the cyclic evolutionary dynamics of the detuned driven Kerr Hamiltonian. (d) Experimentally measured Wigner functions of the cavity state at the origin point in phase space as a function of the evolution time  $t$  and the drive amplitude  $\Omega_d$ . (e) Quantum evolution period extracted from (d) as a function of the drive strength  $\Omega_d$ , exhibiting good agreement with the simulation results (solid line). The yellow dashed line is a fitting of the conjectured function  $T_c = aK^{-1/3}\Omega_d^{-2/3} + b$  with fitting parameters  $a = 3.9$  and  $b = 0.14$ .

To investigate the cyclic quantum dynamics behavior of the detuned driven Kerr Hamiltonian, we numerically simulate the evolution of the initial coherent state under  $H_d$  by solving the master equation. The simulated cavity state is finally displaced back to the origin in phase space using a reverse displacement operator  $D(-\beta)$ . In addition to the Hamiltonian in Eq. S2, higher-order Kerr nonlinear effects with strengths on the order of a few hertz are also considered in the simulations to ensure accuracy, although they are not explicitly shown here. From the simulation, we extract the expectation values  $\langle (a + a^\dagger)/2 \rangle$  and  $\langle -i(a - a^\dagger)/2 \rangle$  during the evolution and reconstruct the quantum state trajectory of the cavity state in phase space. As shown in Fig. S2(a), the trajectory exhibits cyclic evolution, and the average photon number  $\langle a^\dagger a \rangle$ , depicted in Fig. S2(b), also displays periodic oscillations.

The cyclic evolutionary dynamics are also demon-

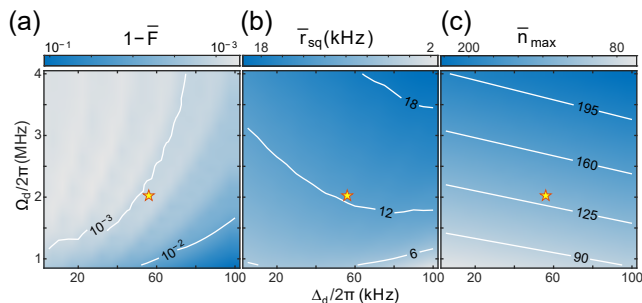


FIG. S3: Numerical simulated average infidelity of the generated squeezed states (a), average squeezing rate (b), and maximum average photon number (c) during the evolution of the cavity state as a function of the frequency detuning  $\Delta_d = \omega_c - \omega_d$  and the drive amplitude  $\Omega_d$  for the first 6 cycles. The star marks the optimal choice of drive parameters for generating the squeezed Fock states in our experiment.

strated experimentally, with the experimental sequence shown in Fig. S2(c). The quantum dynamics of the Wigner function at the origin point in phase space are experimentally measured as a function of the drive strength  $\Omega_d$ . The experimental results shown in Fig. S2(d) indicate that the cyclic period of the quantum state evolution decreases as the drive strength  $\Omega_d$  increases. We extract the evolutionary period  $T_c$  as a function of  $\Omega_d$ , as shown in Fig. S2(e). The experimental results agree well with numerical simulations, indicating the successful modeling of the quantum dynamics of the detuned driven Kerr Hamiltonian. Although it is challenging to derive an analytical expression for  $T_c$ , we could conjecture a possible approximate relationship of  $T_c \propto K^{-1/3} \Omega_d^{-2/3}$  from extensive numerical simulations, which fits well with our measured results in Fig. S2(e). The underlying mechanism of this approximate expression needs further investigation in future work.

To determine the optimal driving parameters for achieving a larger squeezing level, we perform numerical simulations to investigate the performance of the evolved squeezed states after the first six evolution cycles under the Hamiltonian  $H_d$ , while scanning the frequency detuning  $\Delta_d$  and the strength  $\Omega_d$ . In the simulation, the cavity is initialized in a coherent state  $|\beta = 2\rangle$ . Here, the choice of  $\beta = 2$  represents a trade-off that balances the squeezing performance and higher-order Kerr nonlinear effects. A smaller displacement amplitude  $\beta$  results in an insufficient squeezing rate, whereas a larger  $\beta$  amplifies higher-order Kerr nonlinearities, which can deform the squeezed states. We evaluate the average infidelity  $1 - \bar{F}$  of the evolved squeezed states after the first six evolution cycles compared to ideal squeezed states as a function of  $\Delta_d$  and  $\Omega_d$ , with the results shown in Fig. S3(a). The average squeezing rate  $\bar{r}_{sq}$  is also calculated using the squeezing parameters and cyclic periods of the evolution, as shown in Fig. S3(b). Additionally, we extract the maximum average photon number  $\bar{n}_{max}$  of the cavity states during the cyclic squeezing evolution, as shown in

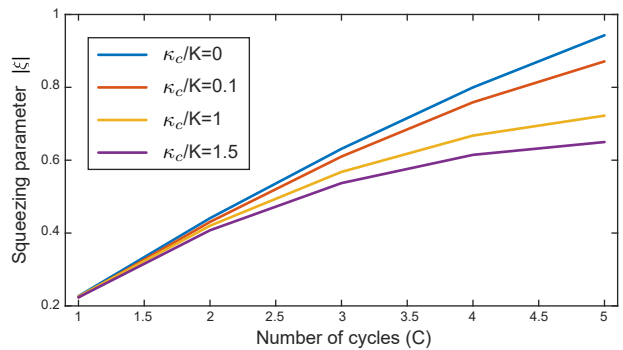


FIG. S4: Numerical simulated squeezing parameters as a function of the evolution cycles for various ratios of  $\kappa_c/K$ .

Fig. S3(c). The simulation results indicate that within the parameter space, higher squeezing rates and fidelities are associated with larger photon numbers during the evolution, which, however, can break the dispersive approximation between the ancillary qubit and the cavity [1], similar to the case discussed in Sec. VII. The optimal driving parameters used in the experiment are chosen by balancing the above three physical quantities  $\bar{n}_{max}$ ,  $r_{sq}$  and  $\bar{F}$  in the simulation. As a result, we choose the drive frequency detuning of  $\Delta_d/2\pi = 56\text{kHz}$  and drive strength of  $\Omega_d/2\pi = 2.01\text{MHz}$  (marked by a star in Fig. S3), which yield a squeezing fidelity  $\bar{F} = 99.89\%$  and an average squeezing rate  $r_{sq}/2\pi = 12.22\text{kHz}$  after the first six evolution cycles in numerical simulation.

Additionally, the demonstrated quantum squeezing amplification method is also applicable in scenarios where the Kerr nonlinearity  $K$  is extremely weak, even smaller than the single-photon decay rate  $\kappa_c$  of the storage cavity mode. To clarify this point, we conduct a numerical simulation that accounts for photon loss effects by solving the master equation:

$$\frac{d\rho}{dt} = -i[H_d, \rho] + \kappa_c \mathcal{D}[a]\rho, \quad (\text{S3})$$

where  $\mathcal{D}[a]\rho = a\rho a^\dagger - 1/2(a^\dagger a\rho + \rho a^\dagger a)$  is the Lindblad dissipative superoperator describing single-photon loss at a rate of  $\kappa_c$ . In the simulation, we vary the ratio of  $\kappa_c/K$  and calculate the squeezing parameters  $|\xi|$  as a function of the number of evolution cycles while adjusting the driving parameters to ensure similar squeezing parameters after the first evolution cycle. The simulation results, shown in Fig. S4, clearly reveal that the squeezing parameter increases with the number of cycles for different ratios of  $\kappa_c/K$ , demonstrating the effectiveness of the squeezing amplification scheme with an extremely weak Kerr nonlinearity.

### III. CALCULATING THE SQUEEZING PARAMETERS

The generated squeezed states at each evolution cycle are characterized by measuring their Wigner functions and comparing them to those of ideal squeezed states. A general squeezed Fock state can be expressed as

$$|\xi, N\rangle = S(\xi)|N\rangle, \quad (\text{S4})$$

where  $S(\xi) = \exp(\frac{\xi^*}{2}a^2 - \frac{\xi}{2}a^{\dagger 2})$  represents the squeezing operator,  $\xi = |\xi|e^{i\varphi}$  is the squeezing parameter with amplitude  $|\xi|$  and phase  $\varphi$ , and  $|N\rangle$  is the multiphoton Fock state with photon number  $N$ . The Wigner function [10] of this state can be written as

$$W(\alpha) = \frac{2}{\pi}(-1)^N e^{-2|\nu|^2} \mathcal{L}_N(4|\nu|^2), \quad (\text{S5})$$

where  $\nu = \cosh(|\xi|)\alpha^* + e^{-i\varphi} \sinh(|\xi|)\alpha$ , and  $\mathcal{L}_N$  denotes the  $N$ -th order Laguerre polynomial function. We use this function to perform a two-dimensional (2D) fit to the measured Wigner functions of the generated squeezed multiphoton Fock states, as depicted in Fig. 3(d) in the main text. In Fig. S5, we present the 2D fitting results for the measured Wigner functions of the generated squeezed Fock states  $|N\rangle$  (with  $N = 0, 1, 2$ , and 6) after the second cycle ( $C = 2$ ). The fitted results agree well with the experimentally measured Wigner functions. The squeezing parameters  $\xi$  of the generated squeezed Fock states are finally extracted from the fitting results.

However, this 2D Wigner function fitting method requires measuring the full Wigner function of the cavity state to ensure a reliable extraction of the squeezing parameter  $\xi$ , and thus is time-consuming in the experiment. Here, we propose to perform a global fit on the

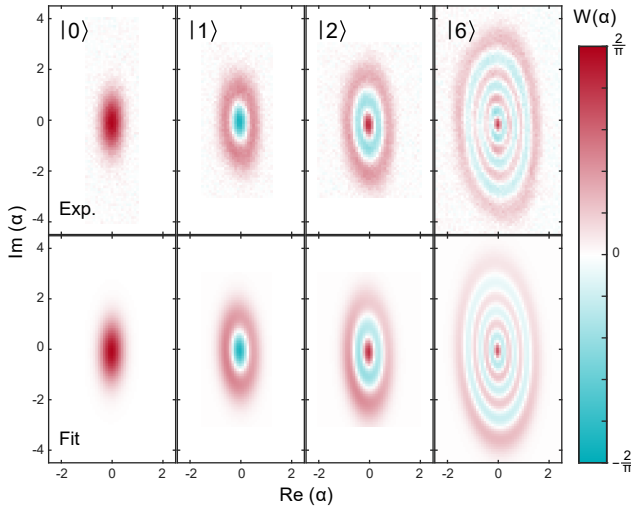


FIG. S5: The measured Wigner functions (up row) and their corresponding 2D fitting results (bottom row) for the generated squeezed Fock states  $|N\rangle$  (with  $N = 0, 1, 2$ , and 6) after the second cycle  $C = 2$ .

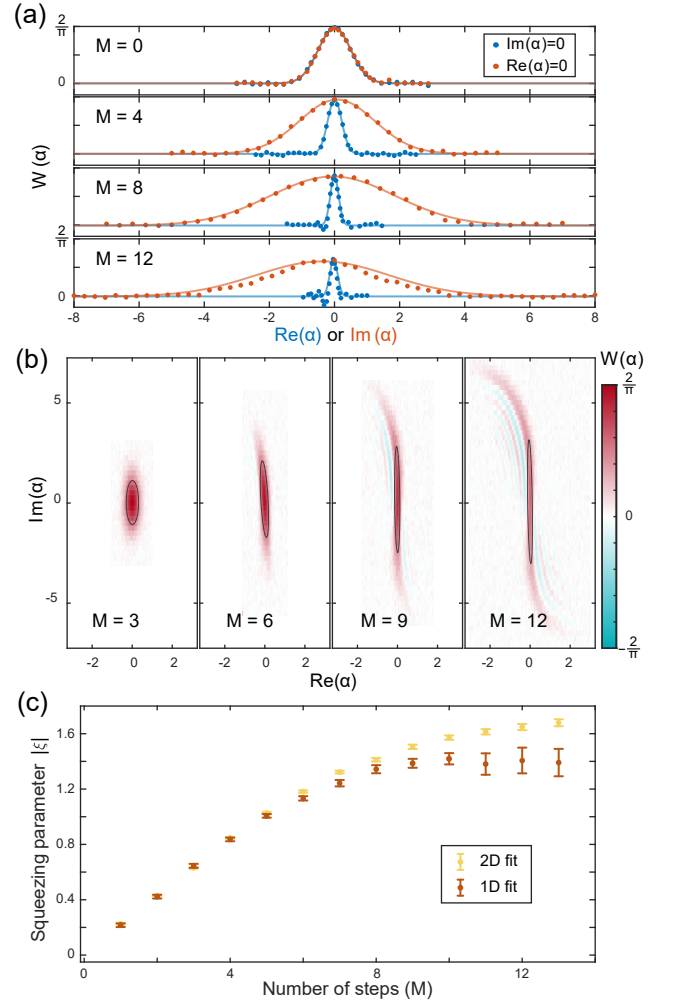


FIG. S6: Measuring squeezing parameters with both 1D and 2D Wigner function fitting methods. **(a)** Measured 1D Wigner function cuts along the real axis (blue symbols) and the imaginary axis (red symbols) for different Trotter steps with  $\beta = 10$ . Solid lines are global fits to the two traces. **(b)** Measured 2D Wigner functions for different Trotter steps with  $\beta = 10$ . The black elliptic lines represent the 2D fitting results. **(c)** Extracted squeezing parameters as a function of the Trotter steps with both the 1D and 2D Wigner function fitting methods shown in (a-b). Error bars are the estimated 95% confidence intervals of the fittings.

one-dimensional (1D) Wigner function cuts along two orthogonal quadratures for the generated squeezed states. In our experiment, we first eliminate the rotation phase  $\varphi$  of the squeezed state according to the method described in Sec. V, and then measure the 1D Wigner function cuts along the real axis ( $\text{Im}(\alpha) = 0$ ) and the imaginary axis ( $\text{Re}(\alpha) = 0$ ), respectively. The ideal expressions for these two 1D Wigner function cuts can be derived as  $W_{sq}(\alpha) = \frac{2}{\pi} \exp(-2e^{2|\xi|}\alpha^2)$  for the squeezing quadrature and  $W_{anti-sq}(\alpha) = \frac{2}{\pi} \exp(-2e^{-2|\xi|}\alpha^2)$  for the anti-squeezing quadrature from Eq. S5. According to these two Gaussian functions, we perform a global fit to the

two measured 1D Wigner function traces to extract the squeezing parameters  $|\xi|$ . Figure S6(a) presents the 1D fitting results of the squeezed states generated using the Trotterization scheme (discussed in Sec. IV) with  $\beta = 10$ .

In addition, we directly measure the full 2D Wigner functions of these generated squeezed states and perform a 2D Wigner function fit, with the fitting results indicated by black elliptical lines in Fig. S6(b). The squeezing parameters extracted from both 1D and 2D Wigner function fitting methods are compared in Fig. S6(c), yielding consistent results for small squeezing. However, for large squeezed states, the fitting results have a little discrepancy because the generated squeezed states exhibit slight deformation and rotation in phase space due to the remaining Kerr and detuning Hamiltonian terms. This leads to fitting errors in the squeezing parameters when using the 1D Wigner function fitting method. The 2D Wigner function fit accounts for residual rotation phases in the fit, thus providing more accurate fitting results for the extracted squeezing parameters.

#### IV. QUANTUM SQUEEZING AMPLIFICATION WITH TROTTERIZATION TECHNIQUE

The quantum evolutionary dynamics of a coherent state  $|\beta\rangle$  under the driven Kerr Hamiltonian  $H_d$  in Eq. S2 can be understood by performing a displacement transformation, resulting in a Hamiltonian:

$$\begin{aligned} H_\beta &= D(-\beta)H_dD(\beta) \\ &= \Delta' a^\dagger a - \frac{K}{2} a^{\dagger 2} a^2 - \frac{K}{2} (\beta^2 a^{\dagger 2} + \beta^{*2} a^2) \\ &\quad - K\beta a^\dagger (a^\dagger a - r) + \text{H.C.}, \end{aligned} \quad (\text{S6})$$

with  $\Delta' = \Delta_d - 2K|\beta|^2$  and  $r = \Delta_d/K + \Omega_d/K\beta - |\beta|^2$  representing the photon-blockade parameter. To completely eliminate the undesired photon-blockade term, we add the driven Kerr Hamiltonian in two opposite displacement frames,  $H_\beta$  and  $H_{-\beta}$ , resulting in the well-known Kerr parametric oscillator Hamiltonian:

$$\begin{aligned} H_{\text{KPO}} &= \frac{H_\beta + H_{-\beta}}{2} \\ &= -\frac{K}{2} (\beta^2 a^{\dagger 2} + \beta^{*2} a^2) \\ &\quad + \Delta' a^\dagger a - \frac{K}{2} a^{\dagger 2} a^2. \end{aligned} \quad (\text{S7})$$

The time evolution of the Hamiltonian  $H_{\text{KPO}}$  can be approximated as

$$\begin{aligned} e^{-iH_{\text{KPO}}T} &= (e^{-i\frac{H_{-\beta} + H_\beta}{2}\delta t})^M \\ &= (e^{-iH_{-\beta}\delta t/2} e^{-iH_\beta\delta t/2})^M \\ &\quad + \mathcal{O}(1/M), \end{aligned} \quad (\text{S8})$$

using the Trotterization technique. Here,  $\delta t = T/M$  is the discretized evolutionary time step, and  $M$  is the number of Trotter steps. The Trotter errors in the first-order

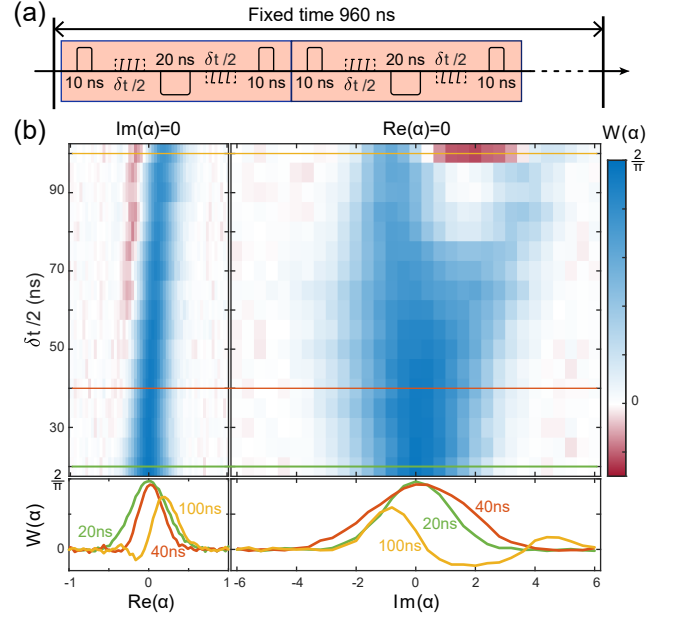


FIG. S7: Calibrating the Trotter time step  $\delta t$ . (a) Experimental sequence with a fixed total evolution time of 960 ns. (b) Measured 1D Wigner function cuts along the real and imaginary axes for various Trotter time steps  $\delta t$  with  $\beta = 8$ . Three horizontal cuts are provided in the bottom row, with  $\delta/2 = 40$  ns (marked by red lines) being used in our experiment in the main text.

Trotter formula of Eq. S8 can be suppressed to an order of  $\mathcal{O}(1/M)$  [11, 12], implying that a smaller time step would reduce the Trotter error.

In our experiment, we calibrate the Trotter time step  $\delta t$  by investigating the performance of quantum squeezing generation using the experimental sequence depicted in Fig. S7(a). In this sequence, the frame transformation displacement operation  $D(\beta)$  has a short pulse duration of 10 ns to suppress Kerr evolution during the frame transformation. For a fixed total evolution time of 960 ns, the measured 1D Wigner function cuts along the real axis ( $\text{Im}(\alpha) = 0$ ) and the imaginary axis ( $\text{Re}(\alpha) = 0$ ) as a function of the Trotter time step  $\delta t$  are shown in Fig. S7(b). The experimental results clearly indicate that a smaller  $\delta t$  would reduce the squeezing degree, while a larger  $\delta t$  would increase the Trotter error. In our experiment, we choose an optimal Trotter time step of  $\delta t = 80$  ns as a trade-off.

To completely eliminate the photon-blockade Hamiltonian term with the Trotterization method, the detuned drive amplitude  $\Omega_d$  in  $H_\beta$  should be changed to  $-\Omega_d$  in  $H_{-\beta}$  for each Trotter step. In our experiment, we set  $\Omega_d = 0$  to limit the average photon number of intermediate states during the evolution and tune the frequency detuning  $\Delta_d$  to partially counteract the accumulated phase induced by the remaining Kerr term. The optimal frequency detunings  $\Delta_d$  for achieving the maximum squeezing parameter for various displacement amplitudes  $|\beta|^2$  are determined from numerical simulations and are pro-

TABLE S2: Optimal frequency detuning  $\Delta_d$  for various  $|\beta|^2$  with the Trotterization method.

$ \beta ^2$	$\Delta_d$ (kHz)
1	6
4	50
16	200
36	350
64	568
100	710

vided in Table S2.

In addition, Trotter errors can be further reduced by utilizing the second-order Trotter formula:

$$\begin{aligned}
 e^{-iH_{\text{KPO}}T} &= (e^{-i\frac{H_{-\beta}+H_{\beta}}{2}\delta t} e^{-i\frac{H_{-\beta}+H_{\beta}}{2}\delta t})^{\frac{M}{2}} \\
 &= (e^{-iH_{\beta}\delta t/2} e^{-iH_{-\beta}\delta t/2} e^{-iH_{-\beta}\delta t/2} e^{-iH_{\beta}\delta t/2})^{\frac{M}{2}} \\
 &\quad + \mathcal{O}(1/M^2)
 \end{aligned} \tag{S9}$$

where Trotter errors are suppressed to the order of  $\mathcal{O}(1/M^2)$  through rearrangement sequence of  $H_{\beta}$  and  $H_{-\beta}$ , as illustrated in Fig. S8(a). We directly perform experimental comparison of the first- and second-order Trotter decomposition schemes and measure the squeezing parameters of generated squeezed vacuum states. The experimental results, shown in Fig. S8(b), indicate almost identical performance for both the first- and second-order Trotter schemes. Therefore, it is unnecessary to adopt a higher-order Trotter scheme [13] in

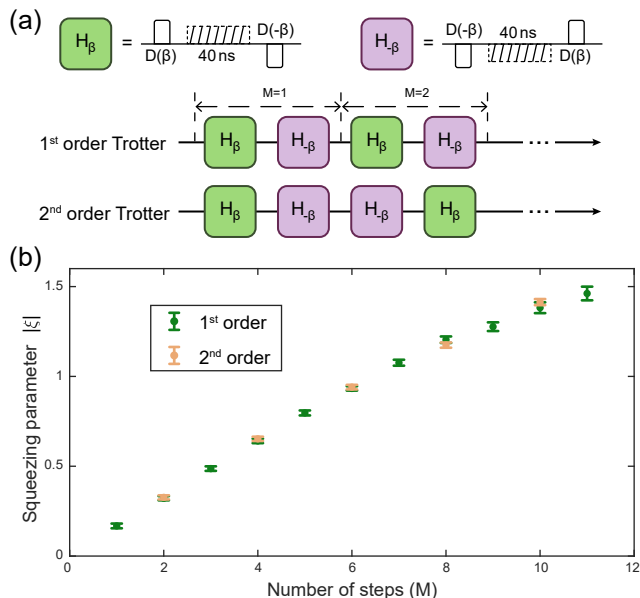


FIG. S8: Comparison of the first- and second-order Trotter schemes. Experimental sequences (a) and the measurement results (b) for both the first- and the second-order Trotter schemes with  $\beta = 8$ . Error bars are the estimated 95% confidence intervals of the 1D fittings.

our experiment, and all experimental results presented in the main text are obtained using the first-order Trotter scheme.

## V. CALIBRATING THE PHASES OF GENERATED SQUEEZED STATES

During the Kerr evolution for generating squeezed state, a rotation phase  $\varphi$  will accumulate due to the remaining Kerr and detuning Hamiltonian terms, resulting in a phase-space inclination of the squeezed states, as illustrated in Fig. S9(a). It is crucial to characterize and eliminate this phase to obtain an accurate squeezing parameter from the 1D Wigner function fit discussed in Sec. III. In our experiment, this phase is calibrated by measuring the Wigner function  $W(\alpha)$  of the generated squeezed state as a function of the rotation phase  $\arg(\alpha)$  with a fixed amplitude  $|\alpha| = 0.7$ . The experimental results are shown in Fig. S9(b) for the generated squeezed states at each Trotter step with  $\beta = 10$ . Subsequently, the rotation phase of the squeezed state at each Trotter step is extracted by identifying the rotation angle that maximizes the Wigner functions. Finally, the calibrated phases of the squeezed states are eliminated by performing virtual phase rotations in the experimental sequence. These virtual operations are implemented by adding a phase offset to the subsequent microwave pulses in the sequence and have a duration of zero [14].

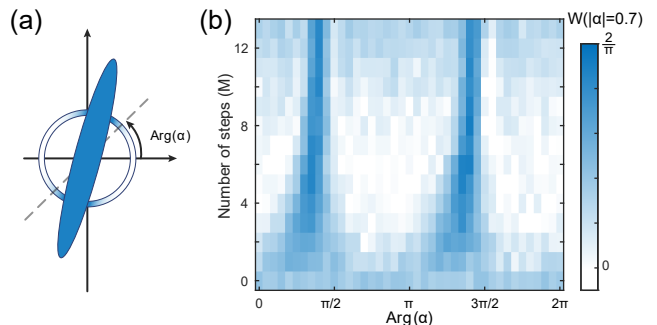


FIG. S9: Calibrating the rotation phases of generated squeezed states. (a) Schematic illustration for calibrating the rotation phases of generated squeezed states. The ring structure indicates the circumferential 1D Wigner functions. (b) Experimentally measured 1D Wigner functions  $W(\alpha)$  as a function of the rotation phase  $\arg(\alpha)$  with a fixed amplitude  $|\alpha| = 0.7$  for various Trotter steps  $M$  with  $\beta = 10$ .

## VI. WIGNER LOGARITHMIC NEGATIVITY AND FISHER INFORMATION

To quantify the nonclassicality and metrological usefulness of the generated squeezed states in our experiment, we calculate the Wigner logarithmic negativity and Fisher information of these nonclassical states from

the reconstructed density matrices. These density matrices are obtained from the measured full Wigner functions using an iterative, convex optimization algorithm [15, 16] based on the maximum likelihood estimation method.

The Wigner logarithmic negativity quantifies the inherent nonclassicality and non-Gaussianity of quantum states [17] and is defined as

$$\delta = \log_2 \left( \int d\alpha |W(\alpha)| \right), \quad (\text{S10})$$

by integrating the absolute values of the Wigner functions of the quantum state over the whole 2D phase space. Although ideal squeezed states are Gaussian states with zero Wigner logarithmic negativity, the squeezed states generated using the Kerr parametric oscillator Hamiltonian with Trotterization method exhibit non-Gaussian features in phase space, thus resulting in large Wigner logarithmic negativities, as illustrated in Fig. 4(e) in the main text.

The Fisher information quantifies the ability to estimate an unknown parameter from the quantum states and serves as a key metric for evaluating the potential of quantum states in quantum metrology. Compared to quasiclassical coherent states, quantum squeezed states have a phase-space structure that is squeezed in one direction and anti-squeezed in the orthogonal direction, making these squeezed states highly sensitive to small displacements along the squeezing direction. The Fisher information for measuring displacement along the position quadrature with squeezed states can be calculated using the formula [18]

$$I_F = \int dx (\partial_x \ln P(x))^2 P(x), \quad (\text{S11})$$

where  $P(x) = \int dp W(\alpha = x + ip)$  represents the position quadrature probability distribution. For an ideal squeezed vacuum state,  $I_F = 4e^{2|\xi|}$ . In Fig. 4(e) in the main text, we compare the Fisher information of the generated squeezed states at various Trotter steps with that of an ideal squeezed state. The results indicate that the extracted Fisher information of the generated squeezed states agrees well with that of the ideal squeezed states. The slight deviation at large squeezing is attributed to a reduction in the purity of the quantum states. Nevertheless, these generated squeezed states remain highly sensitive to small displacements.

## VII. BREAKDOWN OF THE DISPERSIVE APPROXIMATION

In pursuit of a high squeezing rate with the Trotterization technique, a substantial displacement amplitude is required during the displacement frame transformation. However, this leads to excessive photon numbers in the storage cavity, potentially disrupting the dispersive approximation shown in Eq. S1. Consequently, the Jaynes-Cummings (JC) interaction between the storage cavity

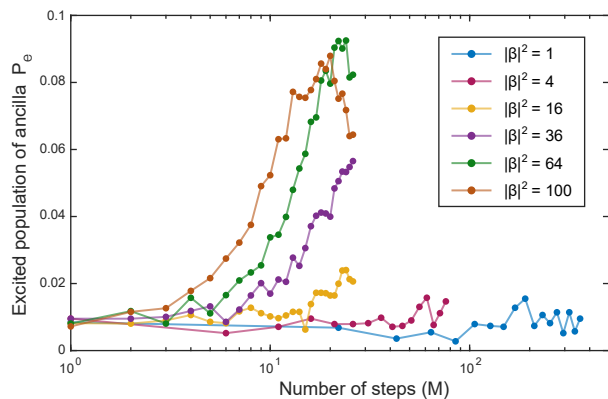


FIG. S10: Excited population of the auxiliary qubit as a function of the number of Trotter steps for various displacement amplitudes  $|\beta|^2$ .

and the ancilla qubit should be considered, as described by the Hamiltonian:

$$H_{\text{JC}} = \omega'_c a^\dagger a + \omega'_q q^\dagger q - \frac{\eta_q}{2} q^{\dagger 2} q^2 + g_{qc} (a^\dagger q + a q^\dagger), \quad (\text{S12})$$

where  $\omega'_c$  and  $\omega'_q$  are their respective bare resonance frequencies and  $g_{qc}$  is the coupling constant between the qubit and the storage cavity. This interaction can induce qubit excitations when the storage cavity contains a large number of photons. This phenomenon is also verified in our experiment by measuring the qubit excited state populations as a number of Trotter steps for various displacement amplitudes  $|\beta|^2$ , with the results depicted in Fig. S10. As the displacement amplitude increases, the qubit excited state population progressively increases with the number of Trotter steps. The breakdown of the dispersive approximation imposes a constraint on the maximum achievable value of  $\beta$  in our experiment. In addition, the qubit excited population induced by the breakdown of the dispersive approximation can diminish the state fidelity of the generated squeezed state because the entanglement between the qubit and the storage cavity during the evolution would reduce the purity of the quantum state in the storage cavity.

## VIII. ERROR ANALYSIS IN THE TROTTER SCHEME

The primary error sources for the displacement-enhanced squeezing generation with Trotterization technique include decoherence errors of the storage cavity, Trotter errors, deformation errors caused by the Kerr nonlinear term, ancillary qubit excitation errors resulting from the breakdown of the dispersive approximation, and errors due to higher-order Kerr nonlinearity. In order to estimate the contributions of these errors, we conduct numerical simulations by solving the master equation while

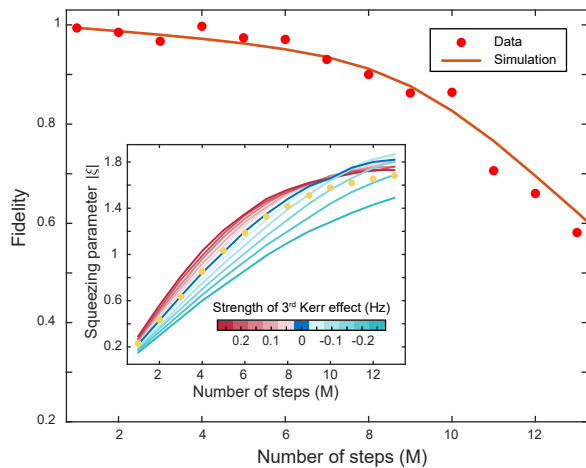


FIG. S11: Error analysis of the generated squeezed states with Trotterization technique. Measured (red circles) and simulated (solid line) state fidelities between the generated quantum states and ideal squeezed states as a function of the Trotter steps. The inset presents the squeezing parameters (yellow circles) extracted from 2D Wigner function fits shown in Fig. S6(c). Solid lines in the inset show the simulation results with varying the third-order Kerr nonlinearity in the simulation.

accounting for these error sources. Figure S11 presents both the simulated and measured state fidelities of the generated squeezed states as a function of Trotter steps with  $\beta = 10$ . The fidelities are determined by comparing the simulated or reconstructed density matrices to the ideal squeezed state. The results indicate that the simulated fidelities are in good agreement with the measure-

ments, demonstrating the effective error modeling in our squeezing generation method. Additionally, we find that the deformation errors induced by Kerr nonlinearity are the predominant errors, which increase with the number of Trotter steps. Potential strategies to mitigate these errors include engineering a quantum harmonic oscillator with ultra-weak Kerr nonlinearity and utilizing large displacement amplitudes, thereby enhancing the squeezing rate while suppressing Kerr deformation errors. We also verify this point in the simulation, where employing a Kerr nonlinearity of  $K/2\pi = 1$  kHz results in a state fidelity exceeding 0.99 with a squeezing parameter  $|\xi| \approx 1.5$ .

Besides, we also provide a comparative analysis of simulated versus experimentally measured squeezing parameters in the inset of Fig. S11 for the generated squeezed states across various Trotter steps. When considering only the first-order ( $\frac{K}{2} a^\dagger 2 a^2$ ) and second-order ( $\frac{K_2}{6} a^\dagger 3 a^3$ ) Kerr nonlinearities in the simulation, we find that the simulation curve of the squeezing parameters increasingly diverges from the experimental results as the Trotter steps increase. This divergence may be attributed to errors induced by higher-order Kerr nonlinearity, such as the third-order Kerr nonlinearity term ( $\frac{K_3}{24} a^\dagger 4 a^4$ ). Here,  $K_2$  and  $K_3$  denote the strengths of the second-order and third-order Kerr effects, respectively. Given that this extremely weak higher-order Kerr nonlinearity is beyond our experimental characterization precision, we investigate its influence by performing numerical simulations with varying the strengths of the third-order nonlinearity. The simulation results shown in the inset capture the behavior of the measured squeezing parameters over the Trotter steps.

- 
- [1] A. Blais, A. L. Grimsmo, S. M. Girvin, and A. Wallraff, “Circuit quantum electrodynamics,” *Rev. Mod. Phys.* **93**, 025005 (2021).
  - [2] Z. Ni, S. Li, X. Deng, Y. Cai, L. Zhang, W. Wang, Z.-B. Yang, H. Yu, F. Yan, S. Liu, C.-L. Zou, L. Sun, S.-B. Zheng, Y. Xu, and D. Yu, “Beating the break-even point with a discrete-variable-encoded logical qubit,” *Nature* **616**, 56 (2023).
  - [3] X. Deng, S. Li, Z.-J. Chen, Z. Ni, Y. Cai, J. Mai, L. Zhang, P. Zheng, H. Yu, C.-L. Zou, S. Liu, F. Yan, Y. Xu, and D. Yu, “Quantum-enhanced metrology with large Fock states,” *Nat. Phys.* **20**, 1874 (2024).
  - [4] M. Reagor, W. Pfaff, C. Axline, R. W. Heeres, N. Ofek, K. Sliwa, E. Holland, C. Wang, J. Blumoff, K. Chou, M. J. Hatridge, L. Frunzio, M. H. Devoret, L. Jiang, and R. J. Schoelkopf, “Quantum memory with millisecond coherence in circuit QED,” *Phys. Rev. B* **94**, 014506 (2016).
  - [5] J. Koch, T. M. Yu, J. Gambetta, A. A. Houck, D. I. Schuster, J. Majer, A. Blais, M. H. Devoret, S. M. Girvin, and R. J. Schoelkopf, “Charge-insensitive qubit design derived from the Cooper pair box,” *Physical Review A* **76**, 042319 (2007).
  - [6] C. Axline, M. Reagor, R. Heeres, P. Reinhold, C. Wang, K. Shain, W. Pfaff, Y. Chu, L. Frunzio, and R. J. Schoelkopf, “An architecture for integrating planar and 3D cQED devices,” *Appl. Phys. Lett.* **109**, 042601 (2016).
  - [7] M. Reagor, H. Paik, G. Catelani, L. Sun, C. Axline, E. Holland, I. M. Pop, N. A. Masluk, T. Brecht, L. Frunzio, M. H. Devoret, L. Glazman, and R. J. Schoelkopf, “Reaching 10 ms single photon lifetimes for superconducting aluminum cavities,” *Appl. Phys. Lett.* **102**, 192604 (2013).
  - [8] Z. Ni, S. Li, L. Zhang, J. Chu, J. Niu, T. Yan, X. Deng, L. Hu, J. Li, Y. Zhong, S. Liu, F. Yan, Y. Xu, and D. Yu, “Scalable Method for Eliminating Residual ZZ Interaction between Superconducting Qubits,” *Phys. Rev. Lett.* **129**, 040502 (2022).
  - [9] G. Kirchmair, B. Vlastakis, Z. Leghtas, S. E. Nigg, H. Paik, E. Ginossar, M. Mirrahimi, L. Frunzio, S. M. Girvin, and R. J. Schoelkopf, “Observation of quantum state collapse and revival due to the single-photon Kerr effect,” *Nature* **495**, 205 (2013).
  - [10] G. M. A. Al-Kader, “Phase distribution from the Wigner function for superpositions of squeezed displaced Fock states,” *J. Opt. B: Quantum Semiclass. Opt.* **5**, S228

- (2003).
- [11] M. Suzuki, “Generalized Trotter’s formula and systematic approximants of exponential operators and inner derivations with applications to many-body problems,” *Commun.Math. Phys.* **51**, 183 (1976).
- [12] J. Han, W. Cai, L. Hu, X. Mu, Y. Ma, Y. Xu, W. Wang, H. Wang, Y. P. Song, C.-L. Zou, and L. Sun, “Experimental simulation of open quantum system dynamics via trotterization,” *Phys. Rev. Lett.* **127**, 020504 (2021).
- [13] M. Suzuki, “Improved Trotter-like formula,” *Phys. Lett. A* **180**, 232 (1993).
- [14] D. C. McKay, C. J. Wood, S. Sheldon, J. M. Chow, and J. M. Gambetta, “Efficient Z gates for quantum computing,” *Phys. Rev. A* **96**, 022330 (2017).
- [15] M. Grant and S. Boyd, “CVX: Matlab software for disciplined convex programming, version 2.1,” <https://cvxr.com/cvx> (2014).
- [16] M. Grant and S. Boyd, “Graph implementations for non-smooth convex programs,” in *Recent Advances in Learning and Control*, Lecture Notes in Control and Information Sciences, edited by V. Blondel, S. Boyd, and H. Kimura (Springer-Verlag Limited, 2008) pp. 95–110, [http://stanford.edu/~boyd/graph\\_dcp.html](http://stanford.edu/~boyd/graph_dcp.html).
- [17] F. Albarelli, M. G. Genoni, M. G. A. Paris, and A. Ferraro, “Resource theory of quantum non-Gaussianity and Wigner negativity,” *Phys. Rev. A* **98**, 052350 (2018).
- [18] A. Eickbusch, V. Sivak, A. Z. Ding, S. S. Elder, S. R. Jha, J. Venkatraman, B. Royer, S. M. Girvin, R. J. Schoelkopf, and M. H. Devoret, “Fast universal control of an oscillator with weak dispersive coupling to a qubit,” *Nat. Phys.* **18**, 1464 (2022).